EDGE ARTICLE

Check for updates

An Fe complex for ^{19}F magnetic resonance-based reversible redox sensing and multicolor imaging†

Rahul T. Kadakia, ‡ Raphael T. Ryan, ‡ Daniel J. Cooke and Emily L. Que *

We report a first-in-class responsive, pentafluorosulfanyl (−SF₅)-tagged ^{19}F MRI agent capable of reversibly detecting reducing environments via an Fe[II/III] redox couple. In the Fe[III] form, the agent displays no ^{19}F MR signal due to paramagnetic relaxation enhancement-induced signal broadening; however, upon rapid reduction to Fe[II] with one equivalent of cysteine, the agent displays a robust ^{19}F signal. Successive oxidation and reduction studies validate the reversibility of the agent. The −SF₅ tag in this agent enables 'multicolor imaging' in conjunction with sensors containing alternative fluorinated tags and this was demonstrated via simultaneous monitoring of the ^{19}F MR signal of this −SF₅ agent and a hypoxia-responsive agent containing a −CF₃ group.

Introduction

Antioxidants, or reducing agents, play a pivotal role in maintaining biological redox balance and counteracting oxidative stress. In a biological setting, common antioxidants include ascorbic acid, which reduces nitrite ions to nitric oxide in the stomach and protects agains reactive oxygen species (ROS); vitamin E, which scavenges free radicals formed during metabolism; and thiol-containing molecules. These thiols, including cysteine and glutathione, help maintain redox balance through their ability to be reversibly oxidized to form disulfides. Reductive stress is a condition in which the cellular redox balance is shifted to a more reducing state. For example, reducing environments are associated with cellular hypoxia, impair signalling functions, promote mitochondrial dysfunction, increase apoptosis, and decrease cell survival.[1,2] Reductive stress is associated with a number of pathologies, including muscular dystrophy, cancer, Alzheimer's disease, rheumatoid arthritis, and alcohol abuse.[3,4]

Many techniques currently exist to detect biological reductants and reducing environments, including positron emission tomography (PET)[5,6] and fluorescence imaging.[7,8] While these are powerful techniques, PET requires the use of ionizing radiation and fluorescence imaging has limited depth penetration for *in vivo* imaging.[9] Thus, alternative techniques that can be readily applied and minimize the use of radioactive materials for *in vivo* sensing are needed. Traditionally, ^{1}H magnetic resonance imaging (MRI) is used to obtain anatomical and physiological images with high temporal resolution and depth penetration without the use of ionizing radiation; however, abundant endogenous ^{1}H signals deriving from water and lipids results in low imaging specificity. As an alternative, fluorine (^{19}F) MRI provides the same excellent depth penetration, and importantly, higher specificity as there is no detectable endogenous fluorine present in the body. Additionally, fluorine-19 is 100% isotopically abundant, and contains high MR receptivity that nears that of [1]H (83% of ^{1}H).[10] In addition to its generally favorable magnetic resonance properties, the ^{19}F nucleus can display MR signals over a broad range of chemical shifts (>350 ppm).[11] A major advantage of molecular MR imaging agents is the exquisite ability to design selective analyte-responsive agents. However, this is partially counterbalanced by high limits of detection on the order of 10^{-4} M or more, which is a barrier to the application of small molecule agents. Regardless, elaborating new mechanisms for MR-based sensing with fluorinated small molecules will inform the development of MR sensors with much greater fluorine density (polymers and other macromolecules, nanoparticles) that provide the fluorine concentrations applicable to *in vivo* detection.

A number of transition metals and lanthanides have been used for redox sensing using magnetic resonance techniques including Eu[II/III], Mn[II/III], Fe[II/III], Co[II/III], and Cu[I/II].[12–37] In order to monitor dynamic redox events in biology, a reversible sensing agent is desirable and this requires a ligand that can effectively cage and sequester a metal ion in two oxidation states. Interest in the use of Fe[II/III] has increased due to the superior biocompatibility of iron relative to other redox active metals and the ability to achieve redox reversibility in biological contexts.[10,30–35] From a magnetic resonance perspective, the differences in electronic relaxation times of the different oxidation states lead to modulation of MR properties, with high spin Fe[III] complexes

Department of Chemistry, University of Texas at Austin, 105 E 24th St. Stop A5300, Austin, TX 78712, USA. E-mail: emilyque@cm.utexas.edu

† Electronic supplementary information (ESI) available: Experimental details and supplementary figures. See DOI: https://doi.org/10.1039/d2sc05222a

‡ These authors contributed equally to this work.

exhibiting substantial ^{19}F MR signal attenuation due to strong paramagnetic relaxation enhancement (PRE) and Fe^{II} complexes exhibiting robust and detectable ^{19}F MR signals due to weak PRE. To the best of our knowledge, while Fe complexes have been reported for ^{19}F MRI applications,[38–45] this is the first demonstration of a reversible, redox-responsive Fe complex for ^{19}F MR biosensing.

Most small molecule ^{19}F MRI agents utilize –CF_3 containing moieties as ^{19}F tags; however, the large ppm range that is available for the ^{19}F nucleus opens up opportunities to design imaging agents with chemical shift values that can be differentiated *via* chemical shift-specific magnetic resonance imaging, enabling 'multicolor' (or chemical shift-selective) imaging of multiple species containing distinct ^{19}F frequencies within the same specimen. The pentafluorosulfanyl (–SF_5) moiety is promising in this respect due to its biostability[46] and distinct chemical shift relative to –CF_3 (~+60 ppm for –SF_5, ~−70 ppm for –CF_3). One disadvantage of an –SF_5 tag is the presence of inequivalent fluorine atoms that reduce signal density and result in doublet (equatorial fluorine atoms) and quintet (axial fluorine atom) signals. Regardless, the value of the –SF_5 tag has been successfully demonstrated in drug tracking studies,[47] though it has never been incorporated for biosensing applications as will be described.

Herein, we report the first Fe-based redox responsive ^{19}F MRI agent, **$Fe^{III}DO3ASF_5$** (Scheme 1), capable of reversibly detecting reducing environments. This agent contains a novel –SF_5 tag that has potential to be used simultaneously alongside a –CF_3 containing agent for multicolor ^{19}F MR imaging.[14]

Results and discussion

$DO3ASF_5$ was synthesized from *$^tBuDO3A$*, chloroacetyl chloride, and 4-(pentafluorosulfanyl)aniline in good yield (48%) following *tert*-butyl ester deprotection (Scheme S1†). The ligand was complexed with anhydrous $FeCl_3$ to obtain **$Fe^{III}DO3ASF_5$** (75%) or with aqueous $Fe(BF_4)_2$ to obtain **$Fe^{II}DO3ASF_5$** (64%).
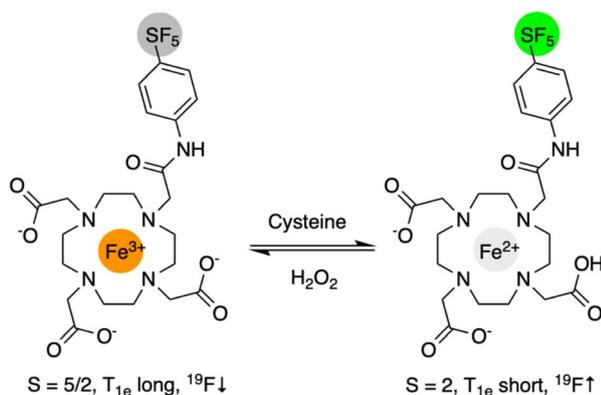
Scheme 1 Design strategy for reversible redox responsive ^{19}F MRI probe exploiting $Fe^{II/III}$ redox chemistry. The initial "off" ^{19}F signal "turns-on" following reduction of Fe^{III} to Fe^{II} by cysteine and "turns-off" following oxidation by H_2O_2. An –SF_5 tag provides a means to simultaneously image these agents with –CF_3 and other ^{19}F-tagged species.

$DO3ASF_5$ and **$Fe^{II/III}DO3ASF_5$** were purified using C18 reverse-phase chromatography. Full details are provided in the ESI.† Previous reports have shown that $Fe^{III}DO3A$ complexes form neutral seven-coordinate complexes derived from three carboxylate and four nitrogen donors.[48] We propose that **$Fe^{III}DO3ASF_5$** forms a similar neutral structure due to its low solubility in water and the one proton difference seen by mass spectrometry between **$Fe^{III}DO3ASF_5$** and **$Fe^{II}DO3ASF_5$**. These observations are reinforced by a remarkable increase in water solubility of **$Fe^{II}DO3ASF_5$**, which would have a water solubilizing free carboxylic acid and only two carboxylate donors directly bound to the metal. The possibility of the amide group also coordinating cannot be ruled out since seven- and eight-coordinate Fe^{II} complexes have been reported.[49–51]

Cyclic voltammetry of 1 mM **$Fe^{III}DO3ASF_5$** in 0.1 M KCl was conducted to characterize the complex's ability to switch between the Fe^{III} and Fe^{II} oxidation states. **$Fe^{III}DO3ASF_5$** displayed a half wave potential, $E_{1/2}$, at 389 mV *vs.* normal hydrogen electrode (NHE, Fig. 1A) with an anodic peak potential, E_{pa}, at 358 mV *vs.* NHE and a cathodic peak potential, E_{pc}, at 420 mV *vs.* NHE, consistent with a reversible redox process. This potential is similar to an $Fe^{III}DOTA$ peptide conjugate reported in the literature ($E_{1/2}$ = 396 mV *vs.* NHE).[52] With an $E_{1/2}$ of 389 mV, both the ferric and ferrous oxidation states of **$FeDO3ASF_5$** should be biologically accessible, as this potential is near that of the one electron reduction of H_2O_2 at pH 7 (380 mV *vs.* NHE).[53] Compared to reversible redox responsive agents for ^1H MRI (FePyC3A $E_{1/2}$ = 230 mV *vs.* NHE,[31] MnHBET $E_{1/2}$ = 356 mV *vs.* NHE),[28] $^1H/^{19}F$ MRI (MnHTFBED $E_{1/2}$ = 250 mV *vs.* NHE),[29] and CEST (CoTPT, $E_{1/2}$ = −107 mV *vs.* NHE),[21] **$Fe^{III}DO3ASF_5$** has a slightly higher potential, indicating our agent favors the reduced state more than these previously reported agents. The cyclic voltammograms of **$Fe^{III}DO3ASF_5$** were similar when the scan speed varied from 50–400 mV s^{-1}, demonstrating the complex is stable and exhibits reversible redox behavior within the given scan speed range.

The absorption spectrum for **$Fe^{III}DO3ASF_5$** displays a characteristic charge-transfer band (extinction coefficient, ε = 3280 M^{-1} cm^{-1}) at 310 nm (Fig. 1B, black trace). The **$Fe^{II}DO3ASF_5$** complex displays a lower absorbance at 310 nm relative to the Fe^{III} complex (Fig. 1B, gray trace). Therefore, we performed an initial screen of different reducing agents and monitored the Fe^{III} to Fe^{II} change using UV-vis spectroscopy. Cysteine, dithiothreitol (DTT), and glutathione (GSH) were selected since they are either commonly used in biological assays (DTT) or because they are biologically relevant agents (cysteine and GSH) that have been shown to reduce other metal MRI agents.[16,54] The initial screening of the three reducing agents showed that DTT and cysteine caused the disappearance of the absorbance peak at 310 nm within 5 minutes. This disappearance is assigned to the reduction of the Fe^{III} complex to Fe^{II} since the resulting absorbance matches the spectrum of **$Fe^{II}DO3ASF_5$** (Fig. 1B and C). In contrast, when 5 equivalents of GSH was used, the reduction was incomplete after 10 minutes (Fig. 1C). However, full reduction was observed when the GSH concentration was increased to 25 equivalents (Fig. S1†). Notably, **$Fe^{III}DO3ASF_5$** was reduced within five minutes by just
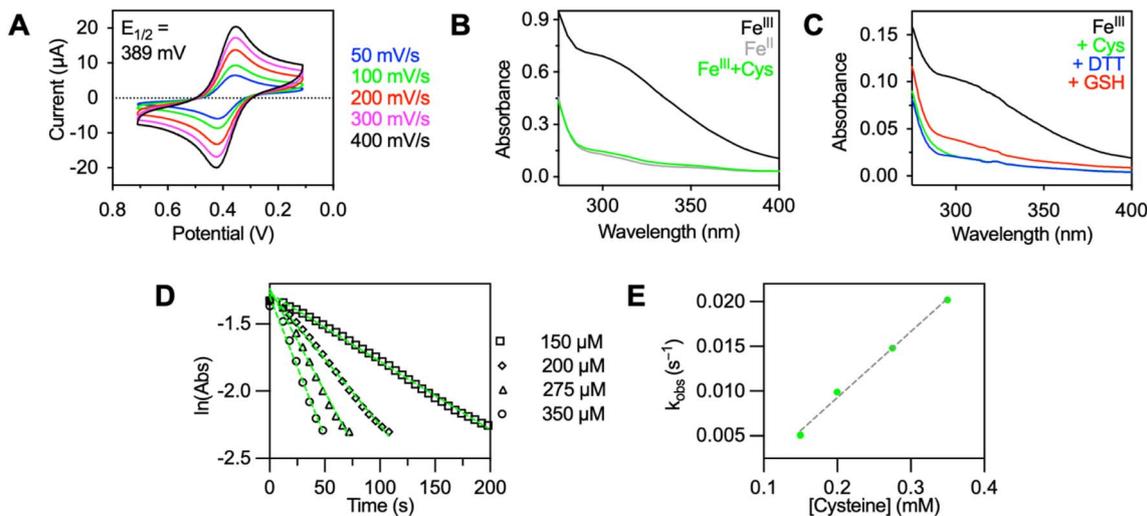
Fig. 1 (A) Cyclic voltammograms of 1 mM $Fe^{III}DO3ASF_5$ in 0.1 M KCl recorded at various scan speeds (50–400 mV s^{-1}). (B) UV-vis absorption spectra of 100 μM $Fe^{III}DO3ASF_5$ in pH 7.4 buffer (black), 100 μM of $Fe^{II}DO3ASF_5$ in pH 7.4 buffer (gray), and 100 μM $Fe^{II}DO3ASF_5$ in pH 7.4 buffer generated in situ from $Fe^{III}DO3ASF_5$ with one equivalent of cysteine (green). (C) UV-vis absorption spectra of 25 μM $Fe^{III}DO3ASF_5$ in deoxygenated pH 7.4 buffer (black) with five equivalents cysteine after five minutes (blue), five equivalents DTT after five minutes (green), and five equivalents of GSH after ten minutes (red). (D) The natural log of the change of absorbance at 310 nm vs. time of the reduction of 25 μM $Fe^{III}DO3ASF_5$ with 150–350 μM of cysteine. Slopes of linear regression fits correspond to the pseudo first-order reaction rates, k_{obs}. (E) Plot of k_{obs} vs. concentration of cysteine, slope of linear regression corresponds to second order rate constant. 5 mM HEPES (pH 7.4) with 10 mM KNO₃ was used for all UV-vis experiments.

one equivalent of cysteine (green trace, Fig. 1B), an improvement over our previously reported macrocyclic Cu^{II}-based sensor that required three equivalents of cysteine for full reduction.[16]

Given the promising reduction results and the biological relevance of cysteine, the kinetics of cysteine-mediated reduction were measured via UV-vis (Fig. S2†). The measurements were determined under pseudo-first order conditions with excess (6–14-fold) cysteine in HEPES buffer (pH 7.4) (Fig. 1D). The reduction is first-order in cysteine and gives a second-order rate constant of $k = 74$ M^{-1} s^{-1} (Fig. 1E). This rate constant is ~50-fold faster than the redox activated ^1H agent, FePyC3A. This is consistent with $Fe^{III}DO3ASF_5$ having a higher $E_{1/2}$ (389 mV compared to 230 mV vs. NHE).[31]

We further characterized these complexes by measuring their solution magnetic moments (μ_{eff}, Evans NMR method).[55,56] $Fe^{III}DO3ASF_5$ exhibited a μ_{eff} of 5.7, consistent with a high spin, $S = 5/2$ Fe^{III} species. With this spin state, we expect strong PRE-induced signal attenuation of the $-SF_5$ tag in this Fe^{III} complex, resulting in the oxidized state being "off" in ^{19}F MR measurements. $Fe^{II}DO3ASF_5$ had a μ_{eff} of 4.5 consistent with a high spin $S = 2$ species.[57] While containing four unpaired electrons, the electronic relaxation times of high spin Fe^{II} species are typically very short, making them inefficient for PRE.[10] Thus we expect to observe significantly less signal broadening for $Fe^{II}DO3ASF_5$ compared to the Fe^{III} complex.

The ^{19}F NMR spectrum of 1 mM $Fe^{II}DO3ASF_5$ in deoxygenated pH 7.4 HEPES (Fig. S3†) contained a severely broadened peak centered at +63.7 ppm with a very low signal-to-noise ratio (SNR). On the other hand, the ^{19}F NMR spectrum of 1 mM $Fe^{II}DO3ASF_5$ contained a doublet at +63.4 ppm (Fig. S4†),

similar to ligand $DO3ASF_5$, which displayed a doublet at +63.2 ppm. The quintet of $Fe^{II}DO3ASF_5$ was not visible even at concentrations as high as 2.5 mM, and therefore, our discussion will focus on the doublet. To confirm that the reduction can be monitored via ^{19}F NMR, 5 equivalents of cysteine were introduced to a sample of $Fe^{III}DO3ASF_5$, which caused the broadened signal to sharpen and increase in intensity, resulting in a doublet at +63.4 ppm, equivalent to that of $Fe^{II}DO3ASF_5$ (Fig. S5†). The relaxation times for $Fe^{II}DO3ASF_5$ alone could not be measured due to the severely broadened nature of its ^{19}F NMR peaks. Given this, the ^{19}F longitudinal (T_1) and transverse (T_2) relaxation times of purified $Fe^{II}DO3ASF_5$ and in situ generated $Fe^{II}DO3ASF_5$ following reduction of $Fe^{III}DO3ASF_5$ were measured at room temperature. $Fe^{II}DO3ASF_5$ had T_1 and T_2 values of 155 and 6.3 ms, respectively. The relaxation times measured for in situ generated $Fe^{II}DO3ASF_5$ ($Fe^{III}DO3ASF_5$ + 5 equivalents DTT) were in strong agreement ($T_1 = 152$ ms, $T_2 = 5.7$ ms).

We next investigated the ability of our complex to reversibly detect environmental redox changes. A 0.5 mM sample of $Fe^{III}DO3ASF_5$ in deoxygenated HEPES was subjected to multiple reduction and oxidation cycles using cysteine and H_2O_2, respectively (Fig. 2). Initially, the 0.5 mM sampled displayed no ^{19}F MR signal (Fig. 2B), exhibited an absorption spectrum consistent with the Fe^{III} species (Fig. 2A), and had the deprotonated $Fe^{III}DO3ASF_5$ mass (ESI$^+$ $m/z = 659$). After adding one equivalent of cysteine, a ^{19}F doublet appeared at +63.4 ppm (Fig. 2B), the Fe^{III} was fully reduced to Fe^{II} according to UV-vis (Fig. 2A), and the protonated $Fe^{II}DO3ASF_5$ mass was observed (ESI$^+$ $m/z = 660$). The same sample was reacted with 10 equivalents of H_2O_2, regenerating $Fe^{III}DO3ASF_5$ which caused

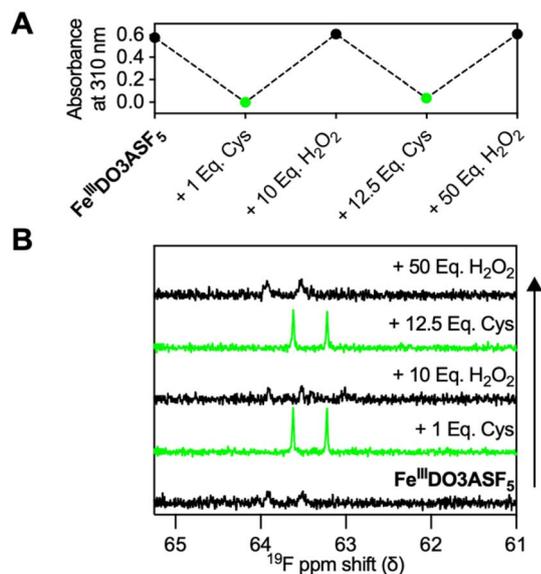**Fig. 2** Repeated reduction and oxidation of **Fe^{III}DO3ASF₅** analyzed via (A) UV-vis (0.1 mM complex, absorbance value at 310 nm) and (B) ^{19}F NMR (0.5 mM) using cysteine ("Cys") and H_2O_2 in 5 mM HEPES buffer (pH 7.4) with 10 mM KNO$_3$.

a broadening in the ^{19}F NMR signal (Fig. 2B), a reappearance of the **Fe^{III}** charge-transfer band (Fig. 2A), and a compound with an m/z of 659. This entire process was repeated multiple times with similar results. Oxidation from **Fe^{II}** to **Fe^{III}** with H_2O_2 occurs rapidly, with complete conversion occurring within 5 minutes in the presence of as low as one equivalent of H_2O_2 as monitored by UV-vis (Fig. S6†).

The kinetic and chemical stabilities of **Fe^{II}DO3ASF₅** and **Fe^{III}DO3ASF₅** were then examined under multiple conditions. The stability of **Fe^{III}DO3ASF₅** was studied in the presence of various biologically relevant metal salts, human serum, and different pH values using UV-vis spectroscopy or ^{19}F NMR. The stability of **Fe^{III}DO3ASF₅** (100 μM) in the presence of different metal salts (100 mM NaCl, 100 mM KCl, 10 mM CaCl$_2$, 10 mM MgCl$_2$, and 100 μM ZnCl$_2$) was monitored before and after incubation by UV-vis (Fig. S7†). The results showed that **Fe^{III}DO3ASF₅** has high stability with no significant absorbance changes observed after 24 h of incubation at 37 °C. Given that **Fe^{III}DO3ASF₅** has a $E_{1/2}$ = 389 mV vs. NHE, it may be sensitive to biological reductants while circulating through the body causing the complex to exist in the Fe^{II} state. If this is the case, the **Fe^{II}DO3ASF₅** complex will dominate, and no selective "turn-on" will be possible. To evaluate this possibility, we monitored **Fe^{III}DO3ASF₅** in human serum (HS) by ^{19}F NMR to estimate its redox sensitivity in that environment. No ^{19}F NMR signal changes were observed for a solution of **Fe^{III}DO3ASF₅** in 80% HS (20% D$_2$O) or 8% HS (20% D$_2$O) in 1X Minimum Essential Medium (MEM) after incubating at 37 °C for 24 h (Fig. S8 and S9†). **Fe^{II}DO3ASF₅** and **Fe^{III}DO3ASF₅** were also stable under acidic (pH 6) conditions as evaluated by ^{19}F NMR (Fig. S10–S12†). The stability of **Fe^{II}DO3ASF₅** under acidic conditions matched well with the in situ generated **Fe^{II}DO3ASF₅** (Fig. S11 and S12†). The stability of **Fe^{II}DO3ASF₅** with metal cations was

determined with ^{19}F NMR due to the low absorbance at wavelengths >300 nm of **Fe^{II}DO3ASF₅** (Fig. S13–S17†). Similar to the **Fe^{III}** complex, **Fe^{II}DO3ASF₅** showed good stability in the presence of abundant metal cations. The air stability of **Fe^{II}DO3ASF₅** was also evaluated in HEPES buffer by UV-vis. Upon exposure to atmospheric oxygen, only minimal absorbance changes were observed over 18 h (Fig. S18†) demonstrating that the complex is relatively stable to oxygen following reduction.

We measured the ^{1}H longitudinal relaxivity (r_1) and transverse relaxivity (r_2) of **Fe^{III}DO3ASF₅** at 60 MHz to gauge the potential presence of an inner sphere water molecule in this complex. The r_1 and r_2 were found to be 0.37 mM^{-1} s^{-1} and 0.39 mM^{-1} s^{-1}, respectively. The r_1 of **Fe^{III}DO3ASF₅** is ~3–22-fold less than many of the previously reported r_1 values for Fe(III) relaxation agents.[58] These lower values are likely because the metal center is coordinatively saturated by the macrocyclic ligand framework and contains no exchangeable protons, which leaves outer-sphere proton relaxation as the only possible mechanism.[59] This coordinatively saturated structure is consistent with the observed high kinetic stability of the complexes.

To validate our –SF$_5$ labelled agent's ability to "turn-on" and be monitored in concert with a –CF$_3$ labelled agent, **Fe^{III}DO3ASF₅** and previously reported hypoxia sensor **CuATSM-F₃** (Fig. S19†)[14] were subjected to ^{19}F MRI using a 7 T scanner. Samples were imaged both at the –SF$_5$ doublet frequency (282.588 MHz) and the –CF$_3$ frequency (282.550 MHz). As shown in Fig. 3, 3 mM **Fe^{III}DO3ASF₅** only provides a signal at the –SF$_5$ frequency when reduced with one equivalent of cysteine (SNR = 25.38); no signal is seen in this sample at the –CF$_3$ frequency (SNR = 1.99). **CuATSM-F₃** was imaged alongside **Fe^{III}DO3ASF₅** to show the agents will only provide signals when reduced and imaged using their respective imaging frequency. Specifically, 5 mM **CuATSM-F₃** displayed a signal when reduced with one equivalent of sodium dithionite (Na$_2$S$_2$O$_4$) using the –CF$_3$ frequency (SNR = 28.92) and no signal when imaged at the –SF$_5$ frequency (SNR = 1.26). We note that **CuATSM-F₃** is unable to provide a "turn-on" response to cysteine, as more reducing
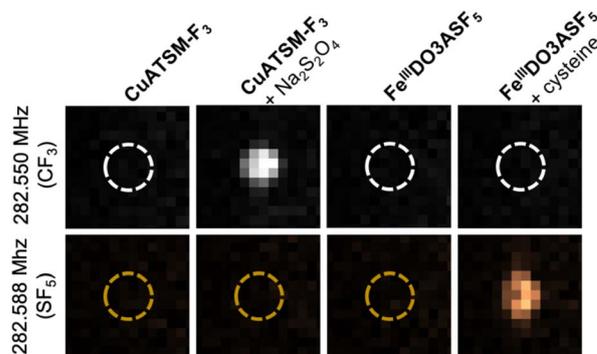

Fig. 3 ^{19}F MRI phantoms of 5 mM **CuATSM-F₃** in the presence and absence of Na$_2$S$_2$O$_4$ and 3 mM **Fe^{III}DO3ASF₅** in the presence and absence of cysteine. Images were obtained at both the –CF$_3$ (282.550 MHz) and –SF$_5$ (282.588 MHz) frequencies. Acquisition time for all images was 15 minutes.

conditions typically associated with severe hypoxia are needed to activate this agent (Fig. S20†). The reversibility of $Fe^{III}DO3ASF_5$ can also be monitored using MR imaging (Fig. S21†) as initially no signal is observed for 3 mM $Fe^{III}DO3ASF_5$ (SNR = 2.04), which then "turns-on" with one equivalent of cysteine (SNR = 25.38), and "turns-off" with hydrogen peroxide (SNR = 3.68). Finally, due to the shorter T_1 of $Fe^{II}DO3ASF_5$, using a rapid acquisition with relaxation enhancement (RARE) pulse sequence we were able to triple the number of averages for the $-SF_5$ image compared to the $-CF_3$ image. This resulted in the Fe complex displaying a similar SNR when compared to reduced $CuATSM-F_3$ even though the fluorine concentration was smaller (12 mM ^{19}F for $Fe^{III}DO3ASF_5$ and 15 mM ^{19}F for $CuATSM-F_3$).

Conclusions

In conclusion, $Fe^{III}DO3ASF_5$ is a redox-responsive ^{19}F MR agent that can undergo reversible redox chemistry and be detected using the distinct ^{19}F frequency associated with the biostable $-SF_5$ moiety. Conversion from a high spin $S = 5/2$ Fe^{III} species to a high spin $S = 2$ Fe^{II} species following cysteine addition provides a mechanism for MR signal "turn-on". Oxidation following addition of H_2O_2 provides a mechanism for signal "turn-off". While these species are physiologically present at micromolar concentrations or below in the extracellular space, and thus may be difficult for detection by MRI, previous work in MRI-based redox imaging suggests a huge potential for monitoring redox environments associated with inflammation or hypoxia using MR imaging agents.[31] In proof-of-concept experiments, we demonstrate that this complex can be imaged in concert with the $-CF_3$ tagged hypoxia-responsive agent $CuATSM-F_3$, opening up possibilities for multiplexed biosensing using ^{19}F MR. Ongoing studies include investigating the effects of ligand structure on Fe redox reactivity and biosensing properties and further development of agents with unique tags for multicolor imaging.

Data availability

This data is archived in the Texas Data Repository, https://dataverse.tdl.org/dataverse/emilyque/.

Author contributions

RTK, RTR, and ELQ designed experiments. RTK, RTR, and DJC performed experiments and characterized compounds. RTK, RTR, DJC, and ELQ all contributed to data analysis and manuscript writing.

Conflicts of interest

There are no conflicts of interest to declare.

Acknowledgements

References

1 D. E. Handy and J. Loscalzo, Responses to reductive stress in the cardiovascular system, *Free Radical Biol. Med.*, 2017, **109**, 114–124.

2 W. Xiao and J. Loscalzo, Metabolic Responses to Reductive Stress, *Antioxid. Redox Signaling*, 2020, **32**, 1330–1347.

3 I. Pérez-Torres, V. Guarner-Lans and M. E. Rubio-Ruiz, Reductive Stress in Inflammation-Associated Diseases and the Pro-Oxidant Effect of Antioxidant Agents, *Int. J. Mol. Sci.*, 2017, **18**, 2098.

4 R. Masia, W. J. McCarty, C. Lahmann, J. Luther, R. T. Chung, M. L. Yarmush and G. Yellen, Live cell imaging of cytosolic NADH/NAD(+) ratio in hepatocytes and liver slices, *Am. J. Physiol.: Gastrointest. Liver Physiol.*, 2018, **314**, G97–G108.

5 A. L. Vāvere and J. S. Lewis, Cu-ATSM: a radiopharmaceutical for the PET imaging of hypoxia, *Dalton Trans.*, 2007, 4893–4902, DOI: 10.1039/b705989b.

6 J. J. Vaquero and P. Kinahan, Positron Emission Tomography: Current Challenges and Opportunities for Technological Advances in Clinical and Preclinical Imaging Systems, *Annu. Rev. Biomed. Eng.*, 2015, **17**, 385–414.

7 Y. Wang, X. Han, X. Zhang, L. Zhang and L. Chen, A high-selectivity fluorescent probe for hypoxia imaging in cells and a tumor-bearing mouse model, *Analyst*, 2020, **145**, 1389–1395.

8 X. Tian, Z. Li, Y. Sun, P. Wang and H. Ma, Near-Infrared Fluorescent Probes for Hypoxia Detection via Joint Regulated Enzymes: Design, Synthesis, and Application in Living Cells and Mice, *Anal. Chem.*, 2018, **90**, 13759–13766.

9 M. L. James and S. S. Gambhir, A molecular imaging primer: modalities, imaging agents, and applications, *Physiol. Rev.*, 2012, **92**, 897–965.

10 D. Xie, M. Yu, R. T. Kadakia and E. L. Que, 19F Magnetic Resonance Activity-Based Sensing Using Paramagnetic Metals, *Acc. Chem. Res.*, 2020, **53**, 2–10.

11 I. Tirotta, V. Dichiarante, C. Pigliacelli, G. Cavallo, G. Terraneo, F. B. Bombelli, P. Metrangolo and G. Resnati, 19F Magnetic Resonance Imaging (MRI): From Design of Materials to Clinical Applications, *Chem. Rev.*, 2015, **115**, 1106–1129.

12 R. T. Kadakia, D. Xie, D. Martinez, M. Yu and E. L. Que, A dual-responsive probe for detecting cellular hypoxia using ^{19}F magnetic resonance and fluorescence, *Chem. Commun.*, 2019, **55**, 8860–8863.

13 R. T. Kadakia, D. Xie, H. Guo, B. Bouley, M. Yu and E. L. Que, Responsive fluorinated nanoemulsions for ^{19}F magnetic resonance detection of cellular hypoxia, *Dalton Trans.*, 2020, **49**, 16419–16424.

14 D. Xie, T. L. King, A. Banerjee, V. Kohli and E. L. Que, Exploiting Copper Redox for ^{19}F Magnetic Resonance-

Based Detection of Cellular Hypoxia, *J. Am. Chem. Soc.*, 2016, **138**, 2937–2940.

15 D. Xie, S. Kim, V. Kohli, A. Banerjee, M. Yu, J. S. Enriquez, J. J. Luci and E. L. Que, Hypoxia-Responsive ^{19}F MRI Probes with Improved Redox Properties and Biocompatibility, *Inorg. Chem.*, 2017, **56**, 6429–6437.

16 J. S. Enriquez, M. Yu, B. S. Bouley, D. Xie and E. L. Que, Copper(II) complexes for cysteine detection using ^{19}F magnetic resonance, *Dalton Trans.*, 2018, **47**, 15024–15030.

17 K. E. Prosser, D. Xie, A. Chu, G. A. MacNeil, B. R. Varju, R. T. Kadakia, E. L. Que and C. J. Walsby, Copper(II) Pyridyl Aminophenolates: Hypoxia-Selective, Nucleus-Targeting Cytotoxins, and Magnetic Resonance Probes, *Chem.–Eur. J.*, 2021, **27**, 9839–9849.

18 N. Kitamura, T. Hiraoka, K. Tanaka and Y. Chujo, Reduced glutathione-resisting ^{19}F NMR sensors for detecting HNO, *Bioorg. Med. Chem.*, 2012, **20**, 4668–4674.

19 M. Yu, D. Xie, R. T. Kadakia, W. Wang and E. L. Que, Harnessing chemical exchange: ^{19}F magnetic resonance OFF/ON zinc sensing with a Tm(III) complex, *Chem. Commun.*, 2020, **56**, 6257–6260.

20 M. Yu, D. Xie, K. P. Phan, J. S. Enriquez, J. J. Luci and E. L. Que, A Co^{II} complex for ^{19}F MRI-based detection of reactive oxygen species, *Chem. Commun.*, 2016, **52**, 13885–13888.

21 P. B. Tsitovich, J. A. Spernyak and J. R. Morrow, A Redox-Activated MRI Contrast Agent that Switches Between Paramagnetic and Diamagnetic States, *Angew. Chem., Int. Ed.*, 2013, **52**, 13997–14000.

22 D. Xie, M. Yu, Z. L. Xie, R. T. Kadakia, C. Chung, L. E. Ohman, K. Javanmardi and E. L. Que, Versatile Nickel(II) Scaffolds as Coordination-Induced Spin-State Switches for ^{19}F Magnetic Resonance-Based Detection, *Angew. Chem., Int. Ed.*, 2020, **59**, 22523–22530.

23 T. Nakamura, H. Matsushita, F. Sugihara, Y. Yoshioka, S. Mizukami and K. Kikuchi, Activatable ^{19}F MRI Nanoparticle Probes for the Detection of Reducing Environments, *Angew. Chem., Int. Ed.*, 2015, **54**, 1007–1010.

24 L. A. Basal, M. D. Bailey, J. Romero, M. M. Ali, L. Kurenbekova, J. Yustein, R. G. Pautler and M. J. Allen, Fluorinated Eu^{II}-based multimodal contrast agent for temperature- and redox-responsive magnetic resonance imaging, *Chem. Sci.*, 2017, **8**, 8345–8350.

25 L. A. Ekanger, L. A. Polin, Y. Shen, E. M. Haacke, P. D. Martin and M. J. Allen, A Eu(II)-Containing Cryptate as a Redox Sensor in Magnetic Resonance Imaging of Living Tissue, *Angew. Chem., Int. Ed. Engl.*, 2015, **54**, 14398–14401.

26 E. M. Gale, C. M. Jones, I. Ramsay, C. T. Farrar and P. Caravan, A Janus Chelator Enables Biochemically Responsive MRI Contrast with Exceptional Dynamic Range, *J. Am. Chem. Soc.*, 2016, **138**, 15861–15864.

27 E. M. Gale, S. Mukherjee, C. Liu, G. S. Loving and P. Caravan, Structure-redox-relaxivity relationships for redox responsive manganese-based magnetic resonance imaging probes, *Inorg. Chem.*, 2014, **53**, 10748–10761.

28 G. S. Loving, S. Mukherjee and P. Caravan, Redox-Activated Manganese-Based MR Contrast Agent, *J. Am. Chem. Soc.*, 2013, **135**, 4620–4623.

29 H. Chen, X. Tang, X. Gong, D. Chen, A. Li, C. Sun, H. Lin and J. Gao, Reversible redox-responsive ^{1}H/^{19}F MRI molecular probes, *Chem. Commun.*, 2020, **56**, 4106–4109.

30 H. Wang, A. Wong, L. C. Lewis, G. R. Nemeth, V. C. Jordan, J. W. Bacon, P. Caravan, H. S. Shafaat and E. M. Gale, Rational Ligand Design Enables pH Control over Aqueous Iron Magnetostructural Dynamics and Relaxometric Properties, *Inorg. Chem.*, 2020, **59**, 17712–17721.

31 H. Wang, V. C. Jordan, I. A. Ramsay, M. Sojoodi, B. C. Fuchs, K. K. Tanabe, P. Caravan and E. M. Gale, Molecular Magnetic Resonance Imaging Using a Redox-Active Iron Complex, *J. Am. Chem. Soc.*, 2019, **141**, 5916–5925.

32 E. M. Snyder, D. Asik, S. M. Abozeid, A. Burgio, G. Bateman, S. G. Turowski, J. A. Spernyak and J. R. Morrow, A Class of Fe^{III} Macrocyclic Complexes with Alcohol Donor Groups as Effective T_1 MRI Contrast Agents, *Angew. Chem., Int. Ed.*, 2020, **59**, 2414–2419.

33 D. Asik, R. Smolinski, S. M. Abozeid, T. B. Mitchell, S. G. Turowski, J. A. Spernyak and J. R. Morrow, Modulating the Properties of Fe(III) Macrocyclic MRI Contrast Agents by Appending Sulfonate or Hydroxyl Groups, *Molecules*, 2020, **25**, 2291.

34 K. Tanaka, N. Kitamura, Y. Takahashi and Y. Chujo, Reversible signal regulation system of ^{19}F NMR by redox reactions using a metal complex as a switching module, *Bioorg. Med. Chem.*, 2009, **17**, 3818–3823.

35 S. Karbalaei, A. Franke, A. Jordan, C. Rose, P. R. Pokkuluri, R. J. Beyers, A. Zahl, I. Ivanović-Burmazović and C. R. Goldsmith, A Highly Water- and Air-Stable Iron-Containing MRI Contrast Agent Sensor for H, *Chem.–Eur. J.*, 2022, e202201179, DOI: **10.1002/chem.202201179**.

36 P. B. Tsitovich, P. J. Burns, A. M. McKay and J. R. Morrow, Redox-activated MRI contrast agents based on lanthanide and transition metal ions, *J. Inorg. Biochem.*, 2014, **133**, 143–154.

37 J. R. Morrow, J. J. Raymond, M. S. I. Chowdhury and P. R. Sahoo, Redox-Responsive MRI Probes Based on First-Row Transition-Metal Complexes, *Inorg. Chem.*, 2022, **61**, 14487–14499.

38 K. Srivastava, E. A. Weitz, K. L. Peterson, M. Marjańska and V. C. Pierre, Fe- and Ln-DOTAm-F12 Are Effective Paramagnetic Fluorine Contrast Agents for MRI in Water and Blood, *Inorg. Chem.*, 2017, **56**, 1546–1557.

39 A. I. Gaudette, A. E. Thorarinsdottir and T. D. Harris, pH-Dependent spin state population and ^{19}F NMR chemical shift via remote ligand protonation in an iron(II) complex, *Chem. Commun.*, 2017, **53**, 12962–12965.

40 A. E. Thorarinsdottir, A. I. Gaudette and T. D. Harris, Spin-crossover and high-spin iron(II) complexes as chemical shift ^{19}F magnetic resonance thermometers, *Chem. Sci.*, 2017, **8**, 2448–2456.

41 A. A. Kislukhin, H. Xu, S. R. Adams, K. H. Narsinh, R. Y. Tsien and E. T. Ahrens, Paramagnetic fluorinated

nanoemulsions for sensitive cellular fluorine-19 magnetic resonance imaging, *Nat. Mater.*, 2016, **15**, 662.

42 A. H. Jahromi, C. Wang, S. R. Adams, W. Zhu, K. Narsinh, H. Xu, D. L. Gray, R. Y. Tsien and E. T. Ahrens, Fluorous-Soluble Metal Chelate for Sensitive Fluorine-19 Magnetic Resonance Imaging Nanoemulsion Probes, *ACS Nano*, 2019, **13**, 143–151.

43 J. Rho, E. Stares, S. R. Adams, D. Lister, B. Leach and E. T. Ahrens, Paramagnetic Fluorinated Nanoemulsions for *in vivo* F-19 MRI, *Mol. Imaging Biol.*, 2020, **22**, 665–674.

44 C. Wang, S. R. Adams, H. Xu, W. Zhu and E. T. Ahrens, β-*D*iketonate-Iron(III) Complex: A Versatile Fluorine-19 MRI Signal Enhancement Agent, *ACS. Appl. Bio. Mater.*, 2019, **2**, 3836–3842.

45 R. T. Ryan, K. M. Scott and E. L. Que, Design Strategies for Responsive Fluorine-19 Magnetic Resonance Probes Using Paramagnetic Metal Complexes, *Analysis Sensing*, 2023, **3**, e202200041.

46 M. V. Westphal, B. T. Wolfstädter, J. M. Plancher, J. Gatfield and E. M. Carreira, Evaluation of tert-butyl isosteres: case studies of physicochemical and pharmacokinetic properties, efficacies, and activities, *ChemMedChem*, 2015, **10**, 461–469.

47 C. Prinz, L. Starke, T. F. Ramspoth, J. Kerkering, V. Martos Riaño, J. Paul, M. Neuenschwander, A. Oder, S. Radetzki, S. Adelhoefer, P. Ramos Delgado, M. Aravina, J. M. Millward, A. Fillmer, F. Paul, V. Siffrin, J. P. von Kries, T. Niendorf, M. Nazaré and S. Waiczies, Pentafluorosulfanyl (SF 5) as a Superior 19 F Magnetic Resonance Reporter Group: Signal Detection and Biological Activity of Teriflunomide Derivatives, *ACS Sens.*, 2021, **6**, 3948–3956.

48 C. A. Chang, L. C. Francesconi, M. F. Malley, K. Kumar, J. Z. Gougoutas, M. F. Tweedle, D. W. Lee and L. J. Wilson, Synthesis, characterization, and crystal structures of M(DO3A) (M = iron, gadolinium) and Na[M(DOTA)] (M = Fe, yttrium, Gd), *Inorg. Chem.*, 1993, **32**, 3501–3508.

49 A. O. Olatunde, C. J. Bond, S. J. Dorazio, J. M. Cox, J. B. Benedict, M. D. Daddario, J. A. Spernyak and J. R. Morrow, Six, Seven or Eight Coordinate Fe(II) , Co(II)

or Ni(II) Complexes of Amide-Appended Tetraazamacrocycles for ParaCEST Thermometry, *Chem.–Eur. J.*, 2015, **21**, 18290–18300.

50 K. Srivastava, G. Ferrauto, V. G. Young Jr, S. Aime and V. C. Pierre, Eight-Coordinate, Stable Fe(II) Complex as a Dual (19)F and CEST Contrast Agent for Ratiometric pH Imaging, *Inorg. Chem.*, 2017, **56**, 12206–12213.

51 X.-H. Bu, W. Chen, Z.-H. Zhang, R.-H. Zhang, S.-M. Kuang and T. Clifford, The first seven-coordinated iron(II) complex with a nitrogen donor set hepta-dentate macrocyclic polyamine ligand and different coordination modes with its cobalt(II) analogue, *Inorg. Chim. Acta*, 2000, **310**, 110–114.

52 J. C. Joyner and J. A. Cowan, Targeted Cleavage of HIV RRE RNA by Rev-Coupled Transition Metal Chelates, *J. Am. Chem. Soc.*, 2011, **133**, 9912–9922.

53 P. M. Wood, The potential diagram for oxygen at pH 7, *Biochem. J.*, 1988, **253**, 287–289.

54 S. M. Pinto, V. Tomé, M. J. F. Calvete, M. M. C. A. Castro, É. Tóth and C. F. G. C. Geraldes, Metal-based redox-responsive MRI contrast agents, *Coord. Chem. Rev.*, 2019, **390**, 1–31.

55 D. F. Evans, The determination of the paramagnetic susceptibility of substances in solution by nuclear magnetic resonance, *J. Chem. Soc.*, 1959, 2003–2005.

56 P. B. Tsitovich, J. M. Cox, J. B. Benedict and J. R. Morrow, Six-coordinate Iron(II) and Cobalt(II) paraSHIFT Agents for Measuring Temperature by Magnetic Resonance Spectroscopy, *Inorg. Chem.*, 2016, **55**, 700–716.

57 C. J. Bond, G. E. Sokolow, M. R. Crawley, P. J. Burns, J. M. Cox, R. Mayilmurugan and J. R. Morrow, Exploring Inner-Sphere Water Interactions of Fe(II) and Co(II) Complexes of 12-Membered Macrocycles To Develop CEST MRI Probes, *Inorg. Chem.*, 2019, **58**, 8710–8719.

58 E. A. Kras, E. M. Snyder, G. E. Sokolow and J. R. Morrow, Distinct Coordination Chemistry of Fe(III)-Based MRI Probes, *Acc. Chem. Res.*, 2022, **55**, 1435–1444.

59 R. B. Lauffer, Paramagnetic metal complexes as water proton relaxation agents for NMR imaging: theory and design, *Chem. Rev.*, 1987, **87**, 901–927.